Effect of Externally Driven Magnetic Islands on Resistive Ballooning Turbulence*)

Seiya NISHIMURA and Masatoshi YAGI[1,2)]

National Institute for Fusion Science, Toki 509-5292, Japan
[1)]*Research Institute for Applied Mechanics, Kyushu University, Kasuga 816-8580, Japan*
[2)]*Japan Atomic Energy Agency, Naka 311-0193, Japan*

(Received 22 December 2010 / Accepted 3 June 2011)

Turbulent transport in the edge region of tokamak plasmas is simulated using a reduced set of magnetohydrodynamic equations. Repetitive and intermittent transport bursts driven by resistive ballooning turbulence with external heating are observed. The effect of a resonant magnetic perturbation (RMP) on turbulent heat transport is examined, where the electromagnetic response of the plasma to the RMP is solved consistently. The penetration of the RMP excites a magnetic island chain and damps the poloidal flow near the magnetic islands. The transport bursts are found to be replaced by more moderate and continuous transport. The change in the transport pattern is associated with the effect of the RMP on nonlinear coupling of fluctuations.

Keywords: resistive ballooning mode, edge-localized mode, resonant magnetic perturbation, magnetic island, electromagnetic effect

DOI: 10.1585/pfr.6.2403119

1. Introduction

The control of turbulent transport is an important issue for magnetically confined fusion plasmas such as tokamaks and helical devices. Repetitive and intermittent transport bursts due to magnetohydrodynamics(MHD) turbulence in the H-mode pedestal region, called edge-localized modes (ELMs), will be a serious problem in future devices. Recently, current coils have been used to apply resonant magnetic perturbations (RMPs), which generate magnetic island chains or a stochastic magnetic layer by forced magnetic reconnection and mitigate or eliminate the ELMs [1].

Early simulation studies showed that oscillation similar to a so-called type-I ELM is driven by competition between destabilization of the pressure-gradient-driven turbulence by external heating and stabilization by flow shear [2]. Concerning the influence of magnetic islands on turbulent transport, the intrinsic tearing instability such as the classical and neoclassical tearing modes has been mainly investigated. This is because research has focused on core confinement properties, and the influence of RMPs has rarely been considered. The electrostatic resistive ballooning mode was recently simulated in the presence of RMPs [3], and the transport bursts were found to be drastically mitigated. However, in the electrostatic model, the influence of RMPs is included as a background magnetic field perturbation, and physical processes associated with a forced magnetic reconnection, such as (1) the screening of RMP penetration by plasma rotation and (2) the excitation of perturbed flows by RMPs, are outside of scope.

The goal of the present study is to consistently simulate the interaction between resistive ballooning turbulence and magnetic islands due to RMPs in the electromagnetic model. In our previous study, we simulated the nonlinear dynamics of intrinsic magnetic islands in the presence of a RMP for single-helicity perturbations [4]. In this study, the simulation code is extended to solve multi-helicity perturbations, and the three-dimensional dynamics of the turbulence is simulated. In addition, we carefully consider edge boundary conditions with the RMP.

2. Model

First, we introduce a conventional set of reduced MHD equations, that model torus plasmas with large aspect ratios by cylindrical plasmas with effective toroidal curvatures [5]. In the model, a quasi-neutral condition between ion and electron densities is considered, and ion and electron temperatures are assumed to be constant. Because we assume constant temperatures, the effect of thermal transport parallel to the magnetic field lines is outside the scope of the model. We select this model mainly because of difficulties in multi-scale simulations in the presence of the spiked eigenfunctions generated by parallel thermal transport. For simplicity, we assume that ion and electron temperatures are equal to each other, and neglect the influence of electron and ion diamagnetic drifts and electron inertia. The vorticity equation, the generalized Ohm's law, the continuity equation, and the equation of parallel ion motion are given respectively by

author's e-mail: nishimura.seiya@lhd.nifs.ac.jp
*) This article is based on the presentation at the 20th International Toki Conference (ITC20).

$$\frac{\mathrm{d}}{\mathrm{d}t}\nabla_\perp^2\phi = \nabla_\parallel j_\parallel + [\Omega, p] + \mu_\perp\nabla_\perp^4\phi, \tag{1}$$

$$\frac{\partial A}{\partial t} = -\nabla_\parallel\phi + \eta_\parallel\left(j_\parallel - j_{\parallel 0}\right), \tag{2}$$

$$\frac{\mathrm{d}p}{\mathrm{d}t} = \hat{\beta}\left([\Omega, \phi] - \nabla_\parallel v_\parallel + \eta_\perp\nabla_\perp^2 p\right), \tag{3}$$

$$\frac{\mathrm{d}v_\parallel}{\mathrm{d}t} = -\nabla_\parallel p + \mu_\parallel\nabla_\perp^2 v_\parallel, \tag{4}$$

with

$$j_\parallel = -\nabla_\perp^2 A,\ \frac{\mathrm{d}}{\mathrm{d}t} = \frac{\partial}{\partial t} + [\phi,\ ],\ \nabla_\parallel = \frac{\partial}{\partial z} - [A,\ ],$$

$$\nabla_\perp = \hat{\boldsymbol{r}}\frac{\partial}{\partial r} + \hat{\boldsymbol{\theta}}\frac{1}{r}\frac{\partial}{\partial\theta},\ [f, g] = \hat{\boldsymbol{z}}\cdot\nabla f\times\nabla g,$$

where f and g are arbitrary variables. The cylindrical coordinate variables (r, θ, z) correspond to the minor radial length, the poloidal phase angle, and the toroidal length in the torus coordinate, respectively, and $(\hat{\boldsymbol{r}}, \hat{\boldsymbol{\theta}}, \hat{\boldsymbol{z}})$ are unit vectors. The time and lengths are normalized as $t/\tau_\mathrm{A} \to t$, $r/a \to r$, $z/R_0 \to z$, with $\tau_\mathrm{A} = R_0/v_\mathrm{A}$, where v_A is the Alfvén velocity, a is the minor radius, and R_0 is the major radius of the torus plasmas. $\nabla_\perp\Omega$ is the effective toroidal curvature of the magnetic field line, where $\Omega = 2r\cos\theta$. The variables $\{\phi, A, p, v_\parallel\}$ denote the electrostatic potential, the vector potential parallel to the ambient magnetic field, the electron (and also ion) pressure and the plasma velocity parallel to the ambient magnetic field, respectively. β is the ratio between the kinetic pressure and the magnetic pressure measured at the plasma center and the coefficient $\hat{\beta}$ is defined by $\hat{\beta} = \beta/(1+\beta)$. The transport coefficients $\{\mu_\perp, \mu_\parallel, \eta_\parallel, \eta_\perp\}$ denote the perpendicular viscosity, the parallel viscosity, the parallel resistivity, and the perpendicular resistivity ($\hat{\beta}\eta_\perp$ is the particle diffusivity), respectively. We assume that these transport coefficients include both classical transport and anomalous effects due to microscopic turbulence.

In the framework of the reduced MHD equations, the arbitrary variable $f = f(r, \theta, z, t)$ can be written as

$$f_0(r) + \sum_{m,n}\tilde{f}_{m,n}(r, t)\exp\left\{i\left(m\theta - nz\right)\right\}, \tag{5}$$

where m is the poloidal mode number and n is the toroidal mode number. The boundary conditions for the perturbation amplitudes are basically given such that $\tilde{f}_{m,n}(0, t) = \tilde{f}_{m,n}(1, t) = 0$ for $(m, n) \neq (0, 0)$ and $\tilde{f}_{0,0}(0, t) = \tilde{f}'_{0,0}(1, t) = 0$, where prime indicates the radial derivative. To introduce RMPs, an edge boundary condition is imposed on the vector potential such that $\tilde{A}_{m',n'}(1, t) = \psi_a$, where (m', n') are the poloidal and toroidal mode numbers of the RMPs, respectively, and the perturbed radial magnetic field at the edge corresponds to $m'\psi_a$. In earlier studies, special treatment for edge boundary conditions was found to be necessary when considering the RMPs to avoid unphysical jumps in perturbations appear at the edge. To avoid the unphysical phenomena, Ref. [6] proposed that the variables should be flux labels at the edge, i.e., $(\nabla_\parallel f)|_{r=1} = 0$. This constraint can be applied to $\{\phi, p, v_\parallel\}$ in the present model. By using the linearized version of the constraint, perturbation amplitudes that have the same mode number as that of the RMPs should satisfy $\tilde{\phi}_{m',n'} = -(k_\theta/\tilde{k}_\parallel)(\phi'_0 + \tilde{\phi}'_{0,0})\psi_a$, $\tilde{p}_{m',n'} = -(k_\theta/\tilde{k}_\parallel)(p'_0 + \tilde{p}'_{0,0})\psi_a$ and $\tilde{v}_{\parallel m',n'} = -(k_\theta/\tilde{k}_\parallel)(v'_{\parallel 0} + \tilde{v}'_{\parallel 0,0})\psi_a$ at the edge boundary, where $k_\theta = m'/r$ is the poloidal wave number, $k_\parallel = m'/q - n'$ is the parallel wave number, q is the safety factor defined by $1/q = -A'_0/r$ and $\tilde{k}_\parallel$ indicates the parallel wave number including the influence of $\tilde{A}_{0,0}$.

In the simulations, the parameters are chosen such that $\beta = 0.01$, $\mu_\perp = 10^{-5}$, $\eta_\parallel = 10^{-5}$, $\hat{\beta}\eta_\perp = 10^{-5}$, and $\mu_\parallel = 10^{-5}$. The initial profiles are given by $\phi_0 = 0$, $q = 2 + 2r^2$, $p_0 = (\beta/\epsilon)(1 - r^2)$, $v_{\parallel 0} = 0$ and $j_{\parallel 0} = (r^2/q)'/r$. The Fourier modes with $0 \le m \le 50$ and $0 \le n \le 25$ are solved in the simulations, where the resonant modes satisfy the condition $2 \le m/n \le 4$ for the present safety factor. For these parameters, the resistive ballooning mode is linearly unstable and the linear growth rate peaks around $m = 30$, whereas dominant modes are around $m = 10$ in the nonlinear stage. The initial amplitude of the vector potential corresponding to the RMP is given by $\tilde{A}_{m',n'}(r, 0) = \psi_a r^{m'}$, which is the same as the ideal MHD solution in the absence of the equilibrium current. To sustain the pressure gradient, which is relaxed by resistive ballooning turbulence, we introduce external heating such that

$$\frac{\partial\tilde{p}_{0,0}}{\partial t} = -\left[\phi, p\right]_{0,0} + \hat{\beta}\left[A, v_\parallel\right]_{0,0} + \eta_\perp\nabla_\perp^2\tilde{p}_{0,0} + S_p, \tag{6}$$

where the subscript '0, 0' denotes the summation of the $(0, 0)$ Fourier components by nonlinear mode coupling and S_p is the heat source given as $S_p = (\beta\gamma_p/\epsilon)\exp\left(-r_1^2/r^2 - r^2/r_2^2\right)$, this heat source profile is proposed in Ref. [7]. In the present study, $\gamma_p = 10^{-2}$, $r_1 = 0.3$, and $r_2 = 0.5$ are considered, and the peak of the heat source is located at $r = \sqrt{r_1 r_2} \approx 0.4$. The selection of a large γ_p allows the pressure gradient to recover several times in the simulations. On the right-hand side (RHS) of Eq. (6), the first and the second terms correspond to the perpendicular transport due to convection and parallel transport by sound waves, respectively. A poloidal flow source is introduced such that

$$\frac{\partial\tilde{v}_{\theta 0,0}}{\partial t} = \frac{1}{r}\int r\left[\phi, \nabla_\perp^2\phi\right]_{0,0}dr + \frac{1}{r}\int r\left[A, j_\parallel\right]_{0,0}dr + \mu_\perp\frac{\partial}{\partial r}\left[\frac{1}{r}\frac{\partial}{\partial r}\left(r\tilde{v}_{\theta 0,0}\right)\right] + \nu\left(\tilde{v}_{\theta 0,0} - V\right), \tag{7}$$

where $\tilde{v}_{\theta 0,0} = -\tilde{\phi}'_{0,0}$ is the poloidal flow velocity and the last term on the RHS of Eq. (7) corresponds to the poloidal flow source. Following Ref. [2], V is given by $V = d\gamma_{\mathrm{E}\times\mathrm{B}}[1 + \tanh\{(r - r_b)/d\}]$, and we choose $\gamma_{\mathrm{E}\times\mathrm{B}} = 2\times10^{-2}$, $r_b = 0.8$, and $d = 5\times10^{-2}$ and $\nu = 10^{-2}$. The magnitude of the shearing rate $\gamma_{\mathrm{E}\times\mathrm{B}}$ chosen here is of the same order as that of the maximum linear growth rate of the resistive ballooning mode.

In the present study, simulations of the resistive ballooning turbulence are examined for two cases: (a) without the RMP and (b) with the RMP for $(m', n') = (3, 1)$ with $\psi_a = 10^{-3}$.

3. Numerical Results

Figure 1 shows the time evolution of heat flux at $r/a = 0.8$, where 'convective' and 'magnetic' indicate heat fluxes associated with the first terms and the second term on the right-hand side (RHS) of Eq. (6), respectively. In both figures, convective heat fluxes dominates. Similarly, the contribution of the third term on the RHS of Eq. (6) is also negligible compared to the first term. Note that convective heat flux in Fig. 1 (a) shows the repetitive bursts similar to ELMs, whereas that in Fig. 1 (b) is somewhat moderate and continuous. The transport bursts in Fig. 1 (a) are caused not by the flow source but by the strong heating. If a smaller heat source is considered, the suppression of the turbulence by the flow shear and the continuous formation of an edge pedestal in the equilibrium pressure may be essential for exciting transport bursts, as shown in Ref. [2].

Figure 2 shows the contours of the helical flux functions for $(m', n') = (3, 1)$. The helical flux function in our normalization is defined as $h_{m',n'} = -(r - r_s)^2/2L_s - \mathrm{Re}[\sum_{m,n} \tilde{A}_{m,n} \exp\{i(m\theta - nz)\}]$, where r_s is the radial position of the rational surface $q = m'/n'$ and L_s is the magnetic shear length at the rational surface normalized by the minor radius. The contour of the helical flux function is identical to the magnitude of the perturbed magnetic field near the rational surface. The magnitude of the RMP is strong enough to excite magnetic islands, as shown in Fig. 2 (b). Therefore, the change in the transport pattern in Fig. 1 is evidently associated with the excitation of the magnetic island chain.

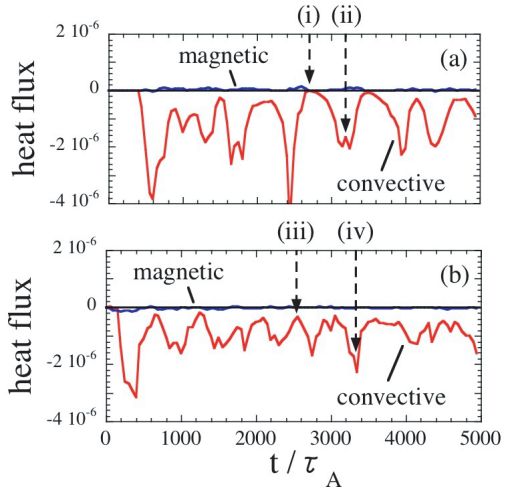

Fig. 1 Time evolution of heat flux (a) without the RMP and (b) with the RMP.

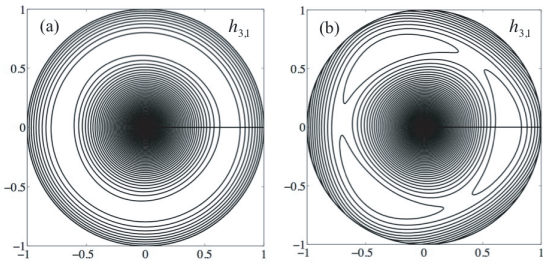

Fig. 2 Contours of the helical flux functions for $(m', n') = (3, 1)$ at $z = 0$ and (a) $t/\tau_A = 3000$ in Fig. 1 (a) and (b) $t/\tau_A = 3000$ in Fig. 1 (b).

Figure 3 shows the electrostatic potential contours. In Fig. 3 (i), the structure is almost concentric, whereas in Fig. 3 (ii) a finger structure is observed. These results confirm that the intermittent transport burst in Fig. 1 (a) is associated with a change of the stability of the resistive ballooning mode. In Figs. 3 (iii) and (iv), perturbations with $m \sim 10$ are observed, which drive moderate transport in Fig. 1 (b). Similar properties are found for the pressure perturbations.

Figure 4 shows the radial profiles of the equilibrium pressure. The global change in the pressure profile in Fig. 4 (a) is associated with the radial propagation of fluctuations from the edge region to the core region. This change is mitigated in Fig. 4 (b). In particular, the pressure profile near magnetic islands is slightly modified. The sustained pressure gradient inside the magnetic islands indicates that perpendicular heat transport is much faster than parallel transport, as shown in Fig. 1.

Figure 5 shows the radial profiles of the equilibrium poloidal flow velocity. The poloidal flow around the O-point is damped, which indicates that the screening effect of the poloidal flow is not strong enough to prevent the penetration of the RMP. The damping of the poloidal flow, i.e. the locking of the poloidal plasma rotation, is explained by the Lorentz torque driven by the interaction between the RMP and the magnetic island chain, which corresponds

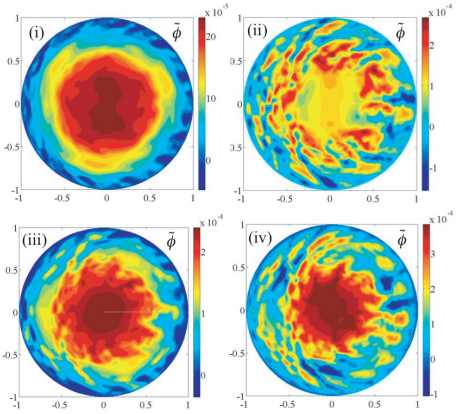

Fig. 3 Contours of the electrostatic potential at $z = 0$. (i) and (ii) are at $t/\tau_A = 2700$, respectively, and $t/\tau_A = 3200$ in Fig. 1 (a), and (iii) and (iv) are at $t/\tau_A = 2550$ and $t/\tau_A = 3350$ in Fig. 1 (b), respectively.

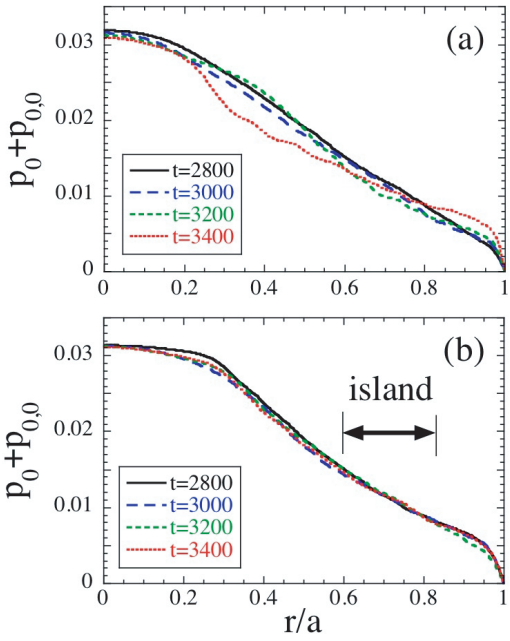

Fig. 4 Radial profiles of the equilibrium pressure (a) without the RMP and (b) with the RMP.

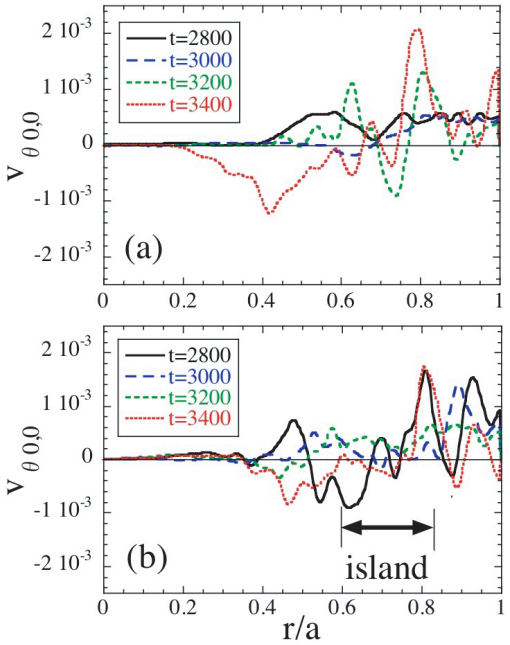

Fig. 5 Radial profiles of the equilibrium poloidal flow velocity (a) without the RMP and (b) with the RMP.

to the second term on the RHS of Eq. (7). Simulations of cases without the poloidal flow $\tilde{v}_{0,0}$ confirm that the existence of the poloidal flow is not essential for the change of the transport pattern observed in Fig. 1.

Figure 6 shows Fourier spectra of convective heat flux, where the modes that contribute to heat transport are identified. In Fig. 6 (b), strong peaks due to $(13,4), (16,5), (17,5)$ and $(20,6)$ are observed simultaneously, whereas $(16,5)$ and $(17,5)$ are weak in Fig. 6 (a).

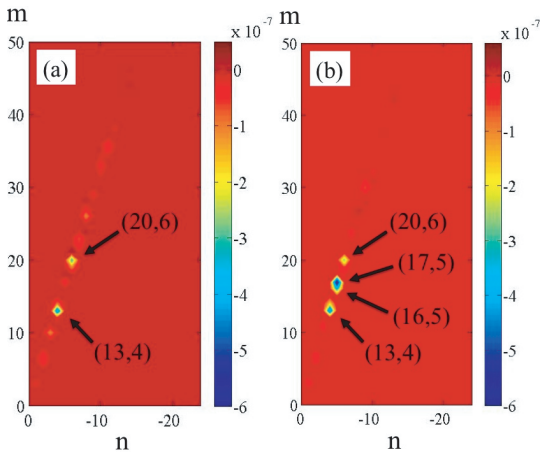

Fig. 6 Fourier mode spectra of convective heat flux (a) without the RMP ($t/\tau_A = 3200$) and (b) with the RMP ($t/\tau_A = 3350$).

This implies that the $(3,1)$ mode due to the RMP plays an important role in the nonlinear coupling of fluctuations excited by the resistive ballooning mode and affects the transport pattern.

4. Summary

In summary, turbulent transport in the presence of a single RMP was simulated, and a change in the transport pattern was observed. Because no flattening of the pressure gradient was observed, the result is *not* understood as the enhancement of heat transport parallel to the reconnected magnetic field lines. Alternatively, it is newly found that the magnetic islands intermediate nonlinear couplings of fluctuations and change the transport properties.

Acknowledgements

This work was partially supported by a Grant-in-Aid for Scientific Research (B) (19360415), the collaboration program of the National Institute for Fusion Science, Japan (NIFS10KTAT048), and the collaboration program of the Research Institute for Applied Mechanics of Kyushu University.

[1] T.E. Evans *et al.*, Phys. Rev. Lett. **92**, 235003 (2004).
[2] P. Beyer, S. Benkadda, G. Fuhr-Chaudier, X. Garbet, Ph. Ghendrih and Y. Sarazin, Plasma Phys. Control. Fusion **49**, 507 (2007).
[3] M. Leconte, P. Beyer, X. Garbet and S. Benkadda, Nucl. Fusion **50**, 054008 (2010).
[4] S. Nishimura, K. Itoh, M. Yagi, K. Ida and S.-I. Itoh, Phys. Plasmas **17**, 122505 (2010).
[5] R.D. Hazeltine, M. Kotschenreuther and P.J. Morrison, Phys. Fluids **28**, 2466 (1985).
[6] F. Militello and F.L. Waelbroeck, Nucl. Fusion **49**, 065018 (2009).
[7] X. Garbet, C. Bourdelle, G.T. Hoang, P. Maget, S. Benkadda, P. Beyer, C. Figarella, I. Voitsekovitch, O. Agullo and N. Bian, Phys. Plasmas **8**, 2793 (2001).